Int. J. Nano Dimens., 13 (4): 414-434, Autumn 2022

ORIGINAL ARTICLE

Green synthesis of rGO/Ag nanocomposite using extracts of *Cinnamomum verum* plant bark: Characterization and evaluation of its application for Methylene blue dye removal from aqueous solutions

Bekele Yirga Mamo, Tegene Desalegn Zeleke*

Department of Applied Chemistry, School of Applied Natural Science, Adama Science and Technology University, P O Box 1888, Adama, Ethiopia

Received 11 July 2022; accepted 04 August 2022; available online 11 August 2022

Abstract

We herein report the green synthesis of a reduced Graphene Oxide/Silver nanoparticle (rGO/AgNP) nanocomposite by simultaneously reduction of graphene oxide and silver ions using an aqueous extract of cinnamon (Cinnamomum verum) plant bark. Methylene blue dye removal capacity and efficiency of the nanocomposite was evaluated. The synthesized nanocomposites were characterized by using UV DRS, SEM, P XRD, and FTIR spectroscopy. The XRD results showed the average particle sizes Ag NPs, rGO, and rGO/Ag NPs nanocomposite to 29.9 nm, 0.67 nm, and 13.35 nm respectively. The UV-DRS analysis result showed that rGO/Ag nanocomposite exhibited two absorbance peaks at 272 & 334 nm which corresponds to rGO and Ag NPs respectively. The FTIR spectral data revealed the functional groups characteristics of phytochemicals in the plant extract, rGO and rGO/AgNP nanocomposite. The surface morphology from SEM result obtained indicated that Ag NPs showed non-homogeneity and different shapes, rGO had thin flat layer sheet morphology whereas Ag NPs were deposited on rGO nanosheets in the form of clusters in the rGO/AgNP nanocomposite. The rGO/AgNP nanocomposite had highest methylene blue removal efficiency of 99.98% at optimum pH 2, adsorbent dose 80 mg, contact time 50 min and initial concentration of 10 mg/l. The Adsorption isotherms were well fitted to Langmuir isotherm for all synthesized adsorbents. The adsorption kinetics results were best fitted to the pseudo-second-order model. The green synthesized rGO/AgNP nanocomposite has the potential to be used as an adsorbent in wastewater treatment applications.

Keywords: *Cinnamon Verum; Green Synthesis; Methylene Blue; Nanocomposite; Reduced Graphene Oxide.*

How to cite this article

Yirga Mamo B., Desalegn Zeleke T. Green synthesis of rGO/Ag nanocomposite using extracts of Cinnamomum verum plant bark: Characterization and evaluation of its application for Methylene blue dye removal from aqueous solutions. Int. J. Nano Dimens., 2022; 13(4): 414-434.

INTRODUCTION

Environmental pollutants are known to cause major problems worldwide. Natural water conservation plays a vital role in protecting the land and saving it for future generations. Textile, papermaking, cosmetics, food, and leather industries release wastewaters into the environment [1]. Among these, the textile industry is one of the major industries as largest water consumer and wastewater source. Wastewater from the textile industry contains chemicals, suspended solids, toxic compounds, and dyestuff, which are among the major pollutants in wastewater. As a result of the rapid development of textile industries, wastewaters containing dyes that are directly or indirectly discharged into the environment are increasing, especially in developing countries. Industrial wastes and their impact on the environment are widely prevalent in Ethiopia, like Addis Ababa and Bahir Dar compared to other parts of the country

* Corresponding Author Email: *tegened@yahoo.com*

This work is licensed under the Creative Commons Attribution 4.0 International License.
To view a copy of this license, visit http://creativecommons.org/licenses/by/4.0/.

[2]. Almost all industries in the city are located in the vicinity of the watercourse and among them; about 90% simply discharge their effluent into the nearby river. This leads to a major impact on the environment, due to toxic substances like heavy metals and dyes discharged into water bodies [3].

Industrial wastewater contains various contaminants, and synthetic dyes are one of the most substantial pollutants in wastewater for their widespread use [4]. Methylene blue (MB) dye is a cationic dye with broad applications such as dye for paper, hair, and cotton and filters for medical surgery among others. It is a pollutant that not only deteriorates water quality but also significantly affects the environment and human health. It has been shown that, in humans, it causes vomiting, lightheadedness, cyanosis, jaundice, tissue necrosis, increased heart rate, vomiting, shock, and tetraplegia [5]. Due to their non-degradability, carcinogenicity, and mutagenicity, eliminating dyes from discharged water is great concern.

Different techniques were used to the removal of these pollutants from contaminated water [6]. Adsorption has some advantages becausetheadsorbentsareinexpensive,areavailable,simple to use, and have high efficiency and their design is simple. Various adsorbents such as silica gel, activated carbon, zeolites etc. have been employed to remove dyes but these adsorbents are not efficient as expected.

Recently, the use of graphene as an adsorbent to solve environmental pollution problems has received considerable attention due to its high specific surface area and unique 2D structure for composite material designing. Several theoretical calculations and experimental measurements were conducted for using graphene as an adsorbent to remove hazardous pollutants from aqueous solutions [7]. Recent literature reports suggest that graphene based composites showed excellent performances for removal of hazardous pollutants. For instance, Supritha *et al*. reported the synthesis of (rGO/MnO_2) composites for removing Hg (II) [8], and in another study Fie, P et.al evaluated $ZnFe_2O_4$/rGO [9] composite for methylene blue dye removal from water. They results indicated that the composites showed enhanced removal capability compared to the parent material. Hence, in water treatment plants, the application of nanomaterials has attracted significant attention because of their large surface areas and more active functionalized sites [4].

In addition metal nanoparticles are among important adsorbents that have drawn considerable attention in recent years because of their [10] appropriate catalytic performance, surface to volume ratio, and considerable controlled porosity [11]. Today, numerous studies have been done about metal nanoparticle biosynthesis and their application in the removal of polluting dyes from wastewaters. For instance, previous studies have different research attempts about the removal of organic dyes using silver nanoparticles [12] and the removal of Rhodamine B using silver nanoparticles, [13]. These particular preferences make it appealing to various applications.

Therefore, composite based nanomaterials are gaining momentum of choice as an adsorbent in water treatment. Currently, the development of green chemistry approaches, which use biomaterials in the synthesis of various nanostructures, has also attracted a considerable amount of attention [14]. The present study was conducted to employ green synthesis to develop an eco-friendly process without any toxic chemicals for the preparation of Ag NPs, rGO, and rGO/Ag NCs and investigate the capacity as well as efficiency of these nanomaterials for methylene blue dye removal from aqueous solution and determine the adsorption isotherm & kinetics model. We assessed the use of cinnamon plant bark (*Cinnamomum Verum*) aqueous extract as a reductant and safe capping agent in an *in situ* reduction procedure for synthesizing Ag NPs on rGO nanosheets. Cinnamon is widely used as a condiment and flavoring agent in cooking [15]. Due to its abundant applications, the commercial production of cinnamon powder is quite high, exhibiting a broader availability for the synthesis of Ag NPs as a biomaterial, and rGO. The aqueous extract of cinnamon was not used previously for composite reduction of rGO/Ag nanocomposites with variable sizes, so we need to use these extract for good production of composite adsorbent rGO/Ag for dye removal. In this work, we used the adsorbent Ag NPs, rGO, and rGO/Ag nanocomposite synthesized using an aqueous extract of cinnamon plant bark, for the removal of methylene blue dye from aqueous solution.

MATERIAL AND METHODS

Chemical and reagents

Most of the chemicals used in this work were analytical grades purchased from Sigma Aldrich (St. Louis, MO, USA), and Merck (Darmstadt, Ger-

CC BY

many) chemical suppliers. The cinnamon plant bark was purchased from Adama town local market. The chemicals used include $AgNO_3$, methylene blue, $NaNO_3$, $KMnO_4$, 98% H_2SO_4, 36% HCl, 30% H_2O_2, NaOH, NH_3, chloroform, graphite powder, distilled water, and tap water.

Experimental Design and Procedures

Preparation of (Cinnamomum verum) bark extract

The preparation of the extract was done using the reported procedure with minor modification. The bark of the cinnamon (*Cinnamomum verum*) plant was ground by using a mortar and pestle to a fine powder. Then 5 gm of cinnamon bark powder was dispersed in 100 mL deionized water in a conical flask and boiled for 45 minutes and later cooled to room temperature. The dispersion was filtered to obtain a clear solution of cinnamon extract and stored in a refrigerator at 4°C until further use [16].

Preparation of graphene oxide (GO)

The graphene oxide was prepared by using the Hummer method with little modification. Accordingly, 5 gm graphite powder and 2.5 gm sodium nitrate were mixed with 120 mL of 98% sulfuric acid in 1000 mL of the conical flask [17]. The mixture was stirred for 30 min in an ice bath followed by the addition of 12 gm potassium permanganate with vigorous stirring at a temperature of below 20°C. The stirring continued overnight and 150 mL of distilled water was slowly added. The reaction temperature was rapidly increased to 98°C and 50 mL of 30% H_2O_2 was added. Then the product sample was washed with 5% HCl, deionized water, and then finally dried.

Reduction of graphene oxide (GO) to reduced graphene oxide (rGO)

To reduce the prepared graphene oxide into reduced form, 3 gm of GO was dispersed in 100 mL distilled water by stirring for a period of 3 h. The suspension was mixed with 50 mL of *Cinnamon verum* plant extract under reflux at 90 ºC for 45 min. The product was also washed with distilled water, dried, and stored [17].

Green synthesis of Ag NPs

The Ag NPs were synthesized by using cinnamon bark extract as the green reducing agent. 50 mL of a clear filtered solution of cinnamon bark extract was added to 100 mL of 0.3M $AgNO_3$ solution stirred at room temperature for 4 h and heated for 30 min at 40-45ºC. The solution color changed from yellow to dark brown was indicating the formation of Ag NPs. The final product was centrifuged at 2000 rpm for 20 min and washed twice with deionized water then finally dried [18].

Synthesis of reduced graphene oxide-silver nanocomposite (rGO/Ag)

Cinnamon bark aqueous extract plays a dual role as a reducing agent for both the graphene oxide (GO) suspension to rGO and silver nitrate ($AgNO_3$) to Ag NP, simultaneously. The GO suspensions are prepared from graphite powder using Hummer's method [17]. 5 gm of the prepared GO and 5 gm of $AgNO_3$ were added in a conical flask, then 100 ml of distilled water was added with continuous stirring on a magnetic stirrer for 2 h at 90 °C, and also 50 ml of cinnamon bark aqueous extract was added which act as a reducing agent and the suspension was stirred continuously for 3 h. UV-Vis spectrophotometric measurements were carried out to confirm the synthesis of the nanocomposite. Later, the sample was centrifuged at 2000 rpm for 10 min and the product powder was dried and stored for further analysis [18].

Phytochemicals tests of cinnamon bark extract

The cinnamon bark extracts were screened for flavonoids, tannins, coumarins, saponosid, glycosides, anthocyanin, terpenoids, and phenols test. The aqueous solution of the sample was prepared according to the method described [19] with little modification and the result clear filtered extract solution was used for coumarins [20], tannins [21], flavonoids [20], saponosid [22], glycosides [21], anthocyanin [21], phenol [22], and terpenoids [22] tests.

Characterization studies

The synthesized rGO, Ag NPs, and rGO/Ag nanocomposite were characterized using various instrumental techniques to confirm the success of the synthetic procedure and to determine the morphologies, particle size, and functional group and other properties required for the material to be used as adsorbent are meeting. In this regard, UV–DRS a Perkin Elmer Lamda-2 spectrophotometer was used for determine the electron transition and bandgap energy (UV-Vis NIR CLB, Model V-770), with a spectral range of 200–800 nm. The crystalline phases of the sample was identified by measuring the intensity of diffraction at 2 the-

(cc) BY

ta angles from 10˚-80˚ using P-XRD (XRD-7000, SHIMADZU Corporation, Japan) equipped with a Cu target for generating a Cu Kα radiation with λ = 0.15406 nm at 40 kV and 50 mA accelerating voltage and applied current respectively. The morphology analysis of the samples was investigated by using SEM (JCM-6000plus BENCHTOP SEM, SHIMADZU Corporation, Japan). The functional groups that are present in the sample detected by using Perkin Elmer-65 model system FTIR-ATR spectrophotometer in the wave number ranging 4000-450 cm^{-1} with a resolution of 2.0 cm^{-1}.

Removal of methylene blue using Ag NPs, rGO, and rGO/Ag NCs by adsorption

Preparation of working standard solutions

In this study, MB powder was used as the adsorbate molecule in adsorption experiments. Preparation of stock solution of MB was carried out by dissolving 1 g of MB in 1000 mL distilled water to get 1000 mg/L. Further 10, 15, 20, and 25 mg/L of working standard solutions of MB were prepared from the standard 1000 mg/L dye solution by using dilution law [23].

Batch adsorption experiment

A batch mode sorption study for individual parameters was carried out using a 250 mL conical flask. The effects of different parameters such as pH, adsorbent dose, adsorbate concentration, and contact time are investigated by varying any one of the parameters and keeping the other parameters constant, and study adsorption isotherms, adsorption kinetics to determine how the change in removal capacity induced by these factors. For each measurement, samples should be periodically taken out of the flask then shaken and filtered using a Whatman filter paper. The investigate ranges of the experimental variables was as follows: pH of solutions (2, 4, 6, 8, & 10), adsorbent dosage (40, 60, 80, 100, 120 mg), initial concentrations (10, 15, 20 & 25 mg/L), and contact time (30, 50, 70, 90 & 110 minutes). The absorbance of the filtrate solutions was determined by using a UV-visible Spectrophotometer at the maximum wavelength of 664 nm and it is possible to calculate the removal efficiency of Ag NPs, rGO, and rGO/Ag NCs by using the Equation 1.

$$\textit{Removal efficiency (\%)} = \frac{Co - Ce}{Co} x100 \quad (1)$$

Where C0 is the initial concentration (mg/L) and Ce is the residual (equilibrium) concentration (mg/L) of the MB being studied.

The removal capacity of rGO/Ag nanocomposite is the amount of MB adsorbed per unit mass of adsorbent was calculated based on the mass balance principle Equation 2.

$$\textit{Removal capacity}\ (qe) = \frac{Co - Ce}{M} x\, v \quad (2)$$

Reusability test of rGO/Ag NPs nanocomposite

80 mg of rGO/Ag nanocomposite was added into 50 ml of MB solution with a concentration of 10 mg/L and then stirred for 50 min. Then the dye adsorbed nanocomposite was separated by centrifugation and desorption carried out by the addition of distilled water. The desorbed nanocomposite was separated and used for the second cycle of adsorption [24]. The same procedure was repeated at least five times to estimate the efficiency of methylene blue dye removal.

Adsorption isotherms

Adsorption isotherms were investigated to evaluate the applicability of the adsorption process for the removal of MB from industrial wastewater. The interactions between the adsorbate and adsorbents also are described by several models for the adsorption isotherms, based on a set of assumptions that are mainly related to the heterogeneity/homogeneity of adsorbents, the type of coverage, and the possibility of interaction between the adsorbate species. The most commonly used equilibrium models are Langmuir and Freundlich isotherms [25]. Therefore, adsorption isotherm experiments were conducted to examine the relationship between the solid phase and the solution phase concentration of the adsorbate at an equilibrium condition.

Langmuir isotherm determined by the following equation (3)

$$\frac{1}{\mathrm{qe}} = \frac{1}{KL\,qmax} * \frac{1}{Ce} + \frac{1}{qmax} \quad (3)$$

Freundlich isotherm determined under the following equation (4)

$$\ln \mathrm{qe} = \ln Kf + \frac{1}{n} * \ln Ce \quad (4)$$

Adsorption kinetic studies

To investigate the adsorption rate processes,

CC BY

the most common models used to fit the kinetic adsorption experiments are pseudo-first-order and pseudo-second-order. The kinetics of adsorption describes the solute uptake rate, which in turn governs the residence time of adsorption reaction [23]. It is one of the important characteristics in defining the efficiency of adsorption.

Pseudo-first order kinetics determined under the following equation (5)

$$\ln(\mathrm{qe}-\mathrm{qt}) = lnqe - K1*t \quad (5)$$

Pseudo-second order kinetics are determined by the following equation (6)

$$\frac{\mathrm{t}}{\mathrm{qt}} = \frac{1}{K2\,\mathrm{qe}^2} + \frac{1}{qe}*t \quad (6)$$

RESULT AND DISCUSSION

Phytochemical screening results

The presence or absence of different phytoconstituents viz. carbohydrate, glycoside, protein, tannins, saponins, flavonoids, and terpenoids were detected by the phytochemical screening methods with different chemical reagents. Phytochemical components are responsible for both pharmacological and toxic activities in plants. These metabolites are said to be useful to a plant itself but can be toxic to animals, including human [26]. The presence of these chemical constituents in this plant is an indication that the plant if properly screened the reducing and capping agent for synthesis of nanoparticles and could yield drugs of pharmaceutical significance.

Flavonoids, tannins, terpenoids, saponin, glycoside, and phenolic compounds were found in cinnamon bark extracts as a good positive result. The coumarins test was slightly positive but anthocyanin was a negative result indicative of its absence in the cinnamon extract. The images showing various color changes during the Phytochemicals screening tests were presented in Fig. 1(a-h) and the summary of the result was tabulated in Table 1. This result is consistent with previous literature reports [21]. Another previous study conducted on an aqueous extract of cinnamon bark reported that tannins, saponins, phenolic, and terpenoids were present, and hence the result of our study was in strong agreement with the reported results of phytochemical screening [27].

Characterization of synthesized adsorbent

X-ray Diffraction analysis (P-XRD)

The crystalline phase structure and orientation of the rGO, Ag NP, and rGO/Ag nanocomposites were studied by XRD analysis at room temperature. Fig. 2 shows a comparison of the XRD patterns of the rGO, Ag NP, and rGO/Ag nanocomposite samples recorded at a diffraction angle in the range 10º–80º. For rGO nanosheets showed a characteristic peak at an angle of 24.73º for the (002) crystal plane. As seen from the figure, the XRD pattern of rGO is not smooth and small peaks were observed. The reason seems to be that there were residual functional groups on the rGO sheets that affected the structure of the rGO sheet. For Ag NPs synthesized (Fig. 2), the diffraction profile had an intense peak at 2θ of 38.29°, 44.30°,

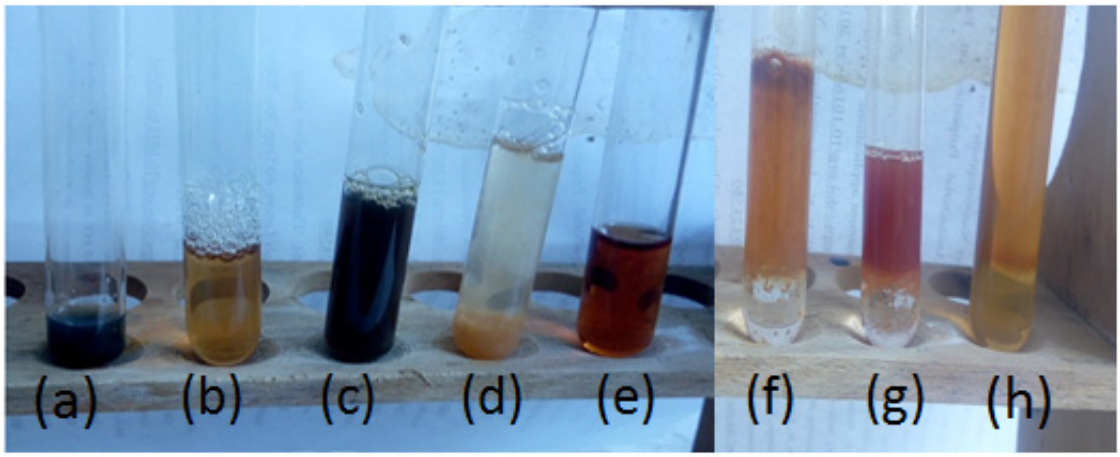

Fig. 1. Phytochemical test result of cinnamon bark extract for (a) phenolic, (b) saponins, (c) tannins, (d) flavonoids, (e) coumarins, (f) glycoside, (g) terpenoids, and (h) anthrocyanin plant constituent metabolites.

Table 1. Qualitative Phytochemical screening of extracts of cinnamon bark.

Plant constituents	Results
Phenolic/ferric chloride test	++
Saponins/frothing test	++
Tannins/ferric chloride test	++
Flavonoids	++
Coumarins/alkaline reagent test	+
Glycoside test	++
Terpenoids/salowski test	++
Anthrocyanin/ammonia test	-

++ High content + moderate content – not found/No content

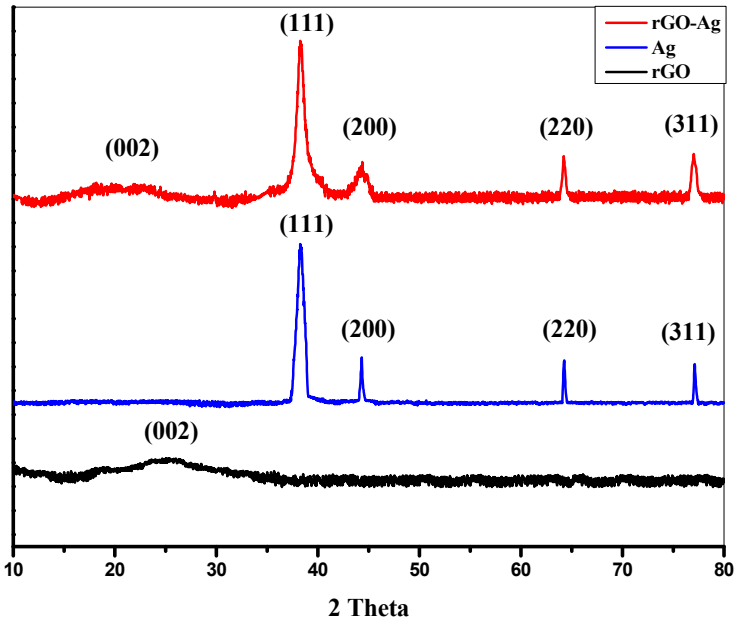

Fig. 2. XRD patterns of rGO, Ag NPs, and rGO/Ag NPs nanocomposite.

64.25°, and 77.12°, corresponding to (111), (200), (220), and (311) planes in Ag NPs reduced by cinnamon bark extract (JCPDS No. 04-0783) [28].

The crystallinity and phase structure of the rGO/Ag NPs nanocomposite also were investigated via XRD analysis. Fig. 2 illustrates the single-phase diffractogram of the material, which signifies that Ag NPs are perfectly embedded over rGO and behave as a single entity. It represents the four significant sharp diffraction peaks at 2θ = 38.32°, 44.27°, 64.23°, and 77.03°, attributed to diffraction over (1 1 1), (2 0 0), (2 2 0), and (3 1 1) planes of the face center cube Ag crystalline phases (JCPDS No. 04-0783). The broad region at 2θ = 20–25° (002) corresponds to the amorphous nature of the rGO moiety (JCPDS No. 84-0713). These obtained results were in good agreement with previously reported literature [29].

The Scherer's equation was applied to calculate each peak crystal size, interlayer distance (d-spacing), and average crystallite size of AgNPs and rGO/AgNPs nanocomposite [30].

$$D = \frac{k\lambda}{\beta cos\theta} \quad (7)$$

Where D is crystallite size, k is Scherer's constant, which is 0.9, λ is the wavelength of the X-ray radiation, which is 0.15406 nm, ß is peak width at half maximum (radians), and θ is Bragg's angle. Hence, the average crystallite size and inter-layer distance (d-spacing) for all samples were calculat-

Table 2. calculated crystallite sizes and interlayer distance (d-spacing) of rGO, Ag NPs, and rGO/Ag NPs nanocomposite from XRD data.

Sample name	2 theta	Theta	d (Aº)	FWHS	D (nm)	D average (nm)
Ag NPs	38.29035	19.14518	2.348742	0.87791	10.00461	29.9nm
	44.30179	22.1509	2.042981	0.30389	28.9024	
	64.25056	32.12528	1.448552	0.21858	40.18277	
	77.12647	38.56324	1.235687	0.21671	40.52951	
rGO/Ag NPs NCs	38.32	19.16	2.346993	1.15552	7.603208	13.35nm
	44.27	22.135	2.044374	1.36506	6.436098	
	64.23	32.115	1.448966	0.37974	23.13599	
	77.03	38.515	1.236994	0.53607	16.38902	
rGO	24.7318	12.3659	3.5969	12.5817	0.67415	0.67415nm

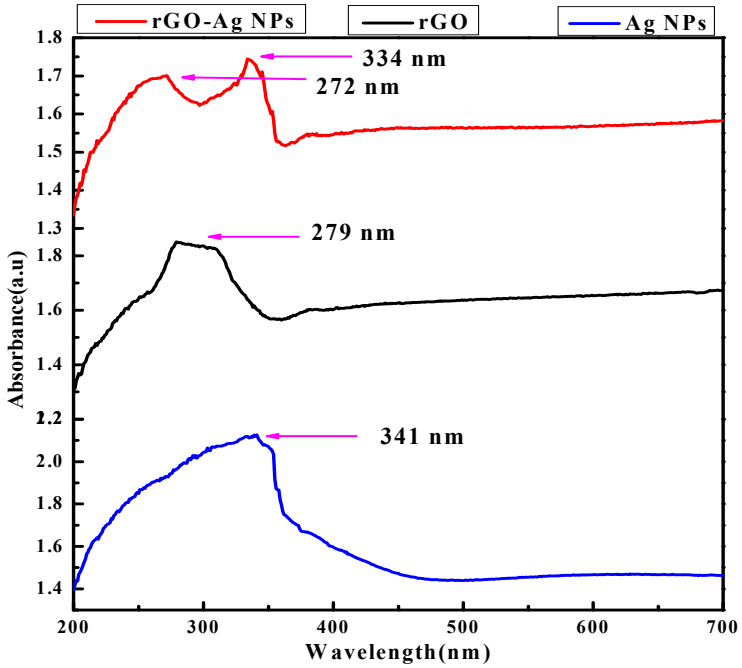

Fig. 3. UV-Vis DRS spectrum of Ag NPs, rGO, and rGO-Ag NCs.

ed and reported in Table 2. Accordingly, the average particle sizes were found to be 29.9 nm, 0.67 nm, and 13.35 nm for Ag NPs, rGO, and rGO/Ag NPs nanocomposite respectively.

UV-DRS Analysis

UV-diffuse reflectance spectroscopy is one of the most widely used techniques for the structural characterization of metal nanoparticles. Due to the unique optical properties of the Ag NPs, a great deal of information about the physical state of the nanoparticles can be obtained by analyzing the optical characterization of Ag NPs. It is known that the size and shape of the Ag NPs considerably change their optical properties since the surface-to-volume ratio increases with a decrease in the size of the particle. Ultraviolet-visible spectroscopy of the silver nanocrystals was performed in a Perkin Elmer Lamda-2 spectrophotometer and the data is shown in Fig. 3. The band detected at 341 nm confirmed that the Ag NPs exhibited different shape and particle size due to non-homogeneity [31]. The reduction of grapheme oxide was confirmed as the solution changed from brown to black color. In addition, the rGO exhibited a peak at 279 nm, which is a red-shift from the characteristic peak of GO at 230–240 nm confirmed the success of the reduction process [32].

The UV-vis spectrum was used to monitor the formation of Ag nanoparticles on the surface of

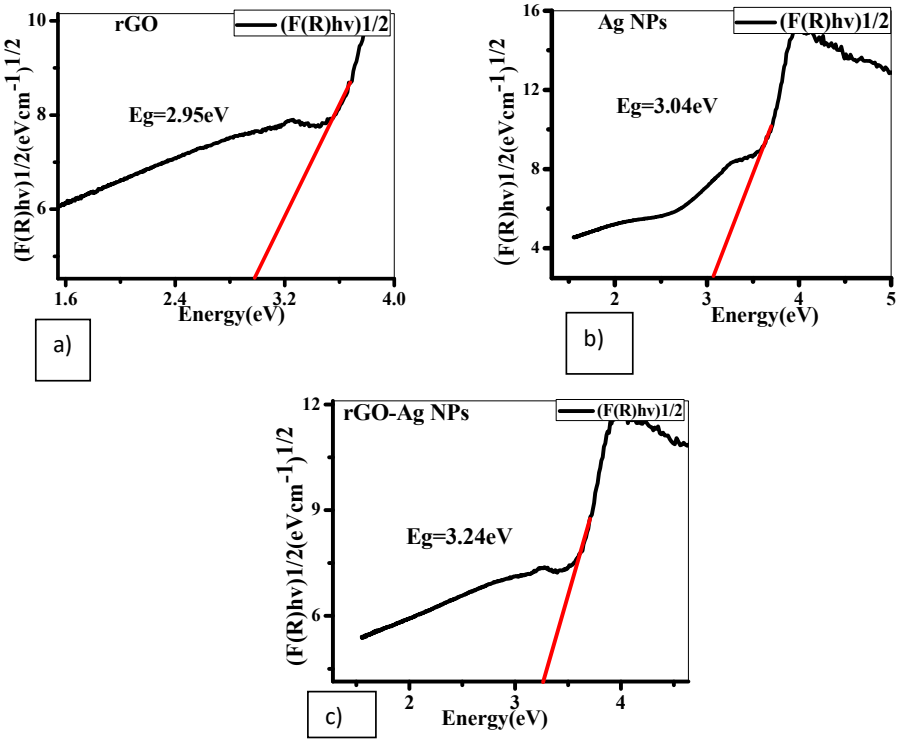

Fig. 4. Band gap energy of a) rGO, b) Ag NPs, and c) rGO-Ag NPs nanocomposite.

graphene. The rGO/Ag nanocomposites showed an obvious blue shift with a sharp peak positioned at 334 nm corresponding to the Ag NPs, where the rGO peak was moved to 272 nm due to the high intense peak arising from the deposition of Ag NPs on the rGO sheets. The blue shift of the plasmonic nanomaterial could be associated with the structure, size as well as properties of the substrate. In addition the observed peak shift could be either due to a decrease in the size of the Ag NPs or due to the presence of rGO, the matrix on which the Ag NPs were deposited [32].

Band gap energy

The diffuse reflectance spectra were translated into the absorption spectra by the Kubelka-Munk method. Kubelka-Munk's equation is described as follows: α =2(1-R)/2R, where α is the absorption coefficient and R is the reflectivity at a particular wavelength.

The bandgap energy can be determined using the Tauc relation. According to the Tauc relation, the absorption coefficient α for material is given by α = A(hv - Eg)n. Where Eg is the bandgap, constant, A is different for different transitions, (hv) is the energy of a photon in eV and n denotes the nature of the sample transition. The 'n' in the equation has values 1/2, 2, 3/2, and 3 for allowed direct, allowed indirect, forbidden direct, and forbidden indirect transitions respectively [33]. The tauc plot of the sample synthesized were presented for rGO (Fig. 4a), Ag NPs (Fig. 4b), and rGO-Ag NPs nanocomposite (Fig. 4c). The data obtained is in agreement with literature report that the optical gap energy of nano-sized crystals depend on their crystallite size; and increases with decreasing crystallite size [34].

The absorption coefficient value is calculated from the diffuse reflectance using Kubelka–Munk equation,

$$F(R) = \frac{2(1-R)}{2R} = K/S \quad (8)$$

Where, R is the absolute reflectance of the Ag NPs, rGO, rGO-Ag NPs nanocomposite, K, is the molar absorption coefficient, and S, is the scattering coefficient. The acquired diffuse reflectance spectrum is converted to Kubelka-Munk function

CC BY

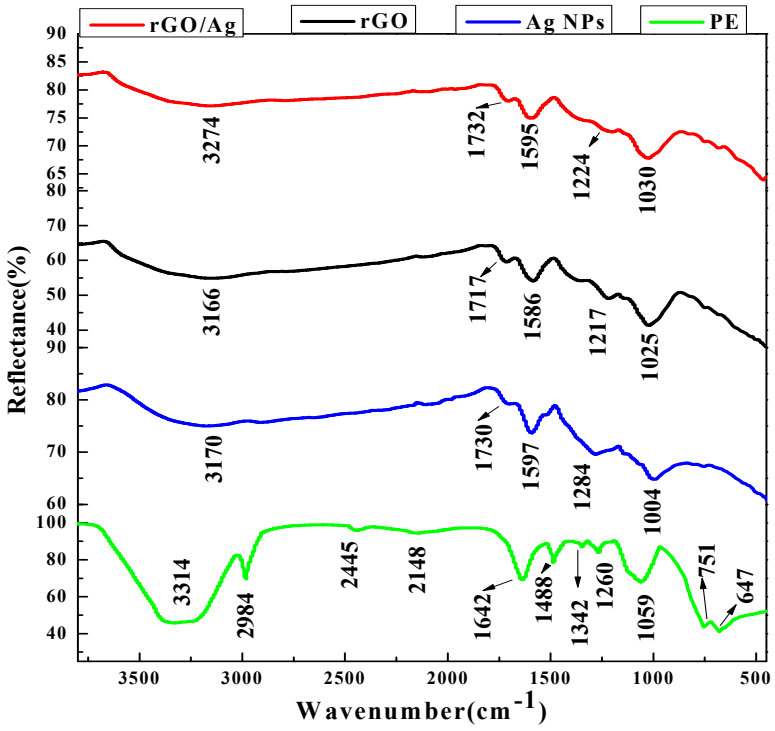

Fig. 5. ATR-FTIR spectrum data of PE, Ag NPs, rGO, and rGO/Ag NPs NCs.

F(R), which is equivalent to the absorption coefficient (α). Thus the vertical axis is converted into the quantity $(F(R)hv)^{½}$ and plotted against photon energy (hv). The indirect allowed $(F(R)hv)^2$ ploted graph result is does not used because its linearity is not fitted with straight line for the curve. In this study the bandgap value is obtained by the intercept of the fitted straight line of the linear part of the curve from $(F(R)hv)^{1/2}$ direct allowed transition. The value of optical band gap energy was found to be 2.95 eV, 3.04 eV, and 3.24 eV for rGO, Ag NPs, and rGO/Ag NPs nanocomposite respectively shown in Fig 4(a-c).

Fourier transform infrared spectroscopy (FTIR-ATR) analysis

FTIR-ATR analysis was employed to evaluate the functional group present in rGO, Ag NPs, rGO/Ag nanocomposite, and cinnamon bark plant extract (PE). The spectra recorded are presented in Fig. 5. Accordingly, due to the fact that green synthesis process utilized cinnamon plant extract, peaks were observed located at around 3314 cm^{-1} corresponding to O-H stretch of alcohol, a peak at 2984 cm^{-1}, (C-H stretch of alkanes), 2445 and 2148 confirms (C≡C stretch of alkynes), and the peak at 1642 cm^{-1} are attributed to the vibration stretching of aldehyde carbonyl (C=O) functional group, representing a high concentration of cinnamaldehyde. Other significant peaks were observed at 647 cm^{-1} (vibration of alkanes), 751 cm^{-1} (benzene rings =CH), 1059 cm^{-1} (C-O), 1260 cm^{-1} (C-O-C bond of aromatic acid ester), 1342 cm^{-1} (C-N stretch, aromatic amines), and 1488 cm^{-1} (C=C bond). All these characteristic peaks confirm that the plant extract is rich in phenolic and aromatic compounds, especially cinnamaldehyde and alcohol.

The dual role of the plant extract as a reducing and capping agent of the functional groups on the NP's surface was confirmed by FTIR analysis. The FTIR spectrum of Ag NPs showed reflectance bands located at 3170, 1730, 1597, 1284, and 1004 cm^{-1} respectively, which correspond to the O-H stretching, C=O stretching, C=C stretching, C-N stretching, and C-C stretching with different functional groups adsorbed on the surface of NPs [35]. Since rGO was synthesized by the reduction of GO, similar peaks were also observed due to the residues of oxy-carboxyl functional groups. It was observed that the peaks in reduced graphene

oxide (rGO) were of weak intensity peaks as compared to graphene oxide at 1025, 1217, 1586, 1717, and 3166 cm^{-1} which corresponds to the C-C, C-O-C, C=C, C=O, and O-H stretching frequencies respectively. When compared to the cinnamon bark extract, the intensity of these peaks was smaller in the spectra of rGO, Ag NPs, and rGO/Ag nanocomposite.

The involvement of cinnamon bark extract as a reducing agent during the reduction could be the source of these hydroxyl groups in rGO and rGO/Ag. In the spectrum obtained from rGO/Ag nanocomposite, the peaks at 3274, 1732, 1595, 1224 and 1030 cm^{-1} show the same pattern of reduced graphene oxide and silver nanoparticles, which exhibited the peak were present O-H stretching, C=O, C=C, C-O-C and C-C stretching respectively by using cinnamon bark extract as reducing and capping agent. The overall FTIR spectra analysis revealed that the synthesis of reduced GO, Ag NPs and rGO/Ag nanocomposite using the cinnamon plant part extract was successful.

Scanning electron microscopy (SEM) analysis

The surface morphology of the synthesized rGO, Ag NPs, and rGO/Ag NP was characterized by using SEM (JEOL, JCM-6000Plus). As shown in Fig. $6a_1$ and Fig. $6a_2$, the synthesized silver nanoparticles indicate that mono-dispersive and demonstrated the non-homogeneity of the particles in terms of their shape and size. It also shows different shapes like spherical, and triangular of Ag NPs with varying particle sizes were found in the micrograph which is a good agreement previously reported literature [36]. The observation of some larger nanoparticles may be attributed to the fact that silver nanoparticles have the tendency to agglomerate due to their high surface energy and high surface tension of the ultrafine nanoparticles [37]. The fine particle size results in a large surface area that, in turn, enhances the nanoparticles' catalytic activity. Fig. 6b1 and Fig. $6b_2$ show that the formed rGO nanosheets were arranged together in stacked sheets, which confirms the reduction of GO. The images revealed an ultra-thin feature of rGO with wrinkles, which suggests the few layers are close together and form an interlinked structure [38].

The SEM images of the rGO/Ag nanocomposite, shown in Fig. $6c_1$ and Fig. $6c_2$, confirmed that Ag nanoparticles are deposited on rGO nanosheets in the form of clusters. The Ag nanoparticles were deposited on rGO nanosheets due to the strong electrostatic and electronic interaction between rGO nanosheets and Ag nanoparticles [39].

Optimization of adsorbent for removal of methylene blue from aqueous solution

In this study we optimized the three synthesized adsorbent rGO, Ag NPs, and rGO/Ag NCs for the removal of methylene blue dye from aqueous solution. The need to optimize the precursor synthesized adsorbent were especially for silver nanoparticles as there is a few previous study for removal of dyes, we need to know the efficiency and capacity by comparing the optimized precursor with the composite efficiency for removal of MB dye as the composites to be expected enhance the removal capability compared to the starting precursor materials.

MB dye adsorption by using Ag NPs, rGO, and rGO/Ag NPs nanocomposite

Effect of pH

The pH of dye solutions plays an important role in the adsorption process and especially in the adsorption efficiency, which is due to the charge of the adsorbent surface, degree of ionization of materials in solution, and also the separation of functional groups in the activated sites of the adsorbent. The influence of pH on the adsorption of dye was studied for three adsorbents separately by adding 80 mg of Ag NPs, rGO, and rGO/Ag NPs to 10 mg/L of methylene blue solution with pH values ranging from 2 to 10 for a contact time of 50 min. As shown in Fig. 7a, dye uptake by Ag NPs increased as the pH of the solution increased because for cationic dyes such as MB, adsorption decreases in pHs lower than pHpzc due to the cationic nature of the adsorbent surface and increases in pHs higher than pHpzc due to the anionic nature of the adsorbent surface [40]. In this study, the adsorption of MB was increased to 10 by increasing pH, and its removal efficiency increased from pH 2 = (86.04%) to pH 10 = (90.03%).

The adsorption of methylene blue dye by rGO and rGO/Ag NPs nanocomposite was found to decrease with an increasing pH value of a solution, as shown in Fig. 7b and Fig. 7c. These show that in an acidic medium, the efficiency of adsorption is greater than in a basic medium. The electrostatic attraction between positively charged H^+ ions that are present in lower pH and cationic charges on the dye is the main reason for the electrostatic ad-

(cc) BY

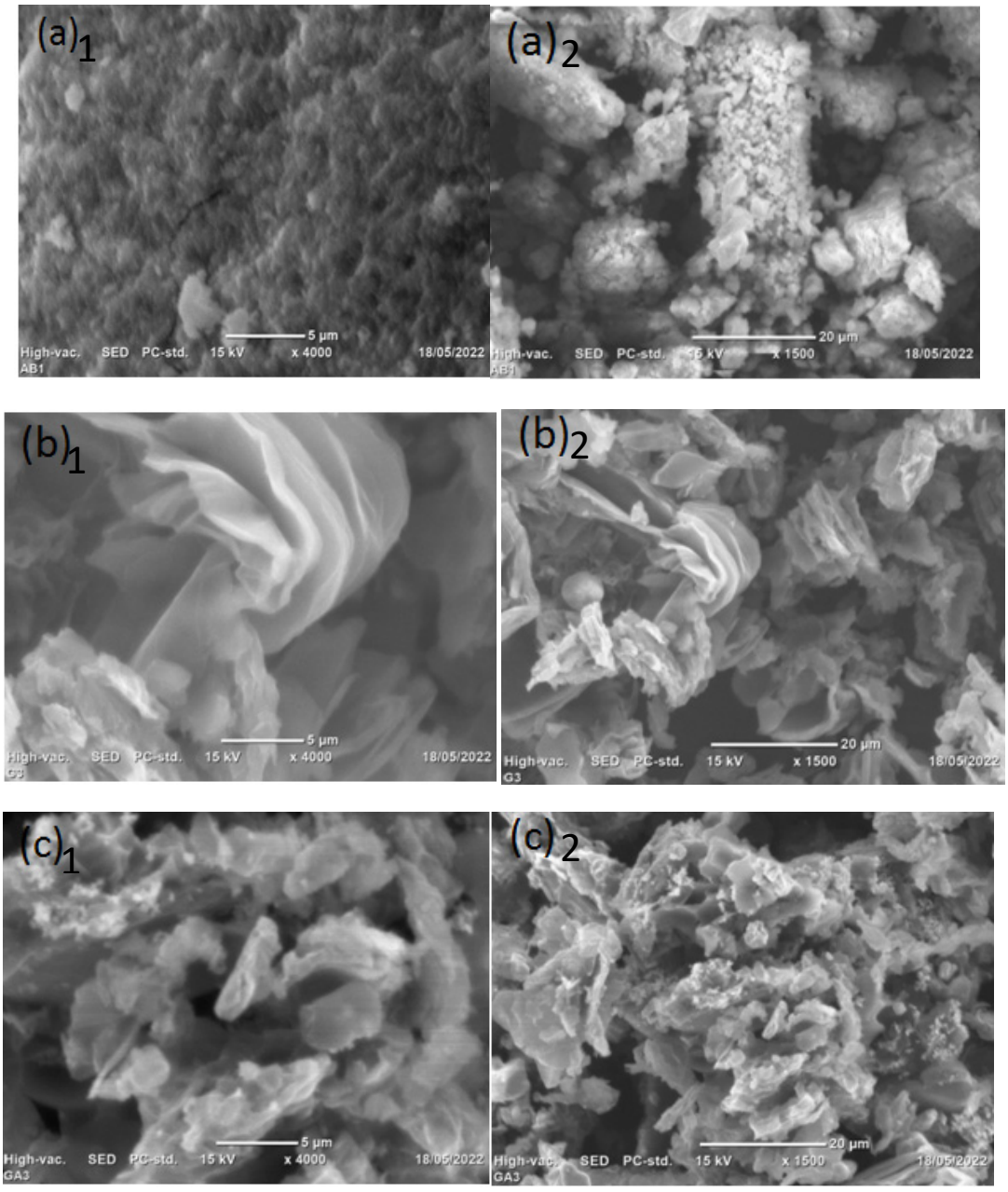

Fig. 6. The SEM analysis of ($a_{1\&2}$) Ag NPs, ($b_{1\&2}$) rGO, and ($c_{1\&2}$) rGO/Ag NPs at different magnification.

sorption. Thus, the optimum pH value for the adsorption of dye using rGO and rGO/Ag nanocomposite is found to be pH 2. The removal efficiency of rGO adsorbent increases from pH 10 = (94.31%) to pH 2 = (96.97%), but the removal efficiency of the two precursor adsorbents is lower than from rGO/Ag nanocomposite. Similarly, in the case of the nanocomposite, the removal efficiency also increased from pH 10 = (97.39%) to pH 2 = (99.98%).

Effect of adsorbent dosage

To study the effect of adsorbent dosage of Ag NPs, at pH 10, rGO at pH 2, and rGO/Ag NPs nanocomposite at pH 2 with time of 50 minutes, and 10 mg/L fixed concentration of MB dye was used. The adsorbent with different doses for each of the three synthesized samples separately (40–120 mg) was used for this experiment. The impact of the adsorbent doses on the elimination effectiveness

CC BY

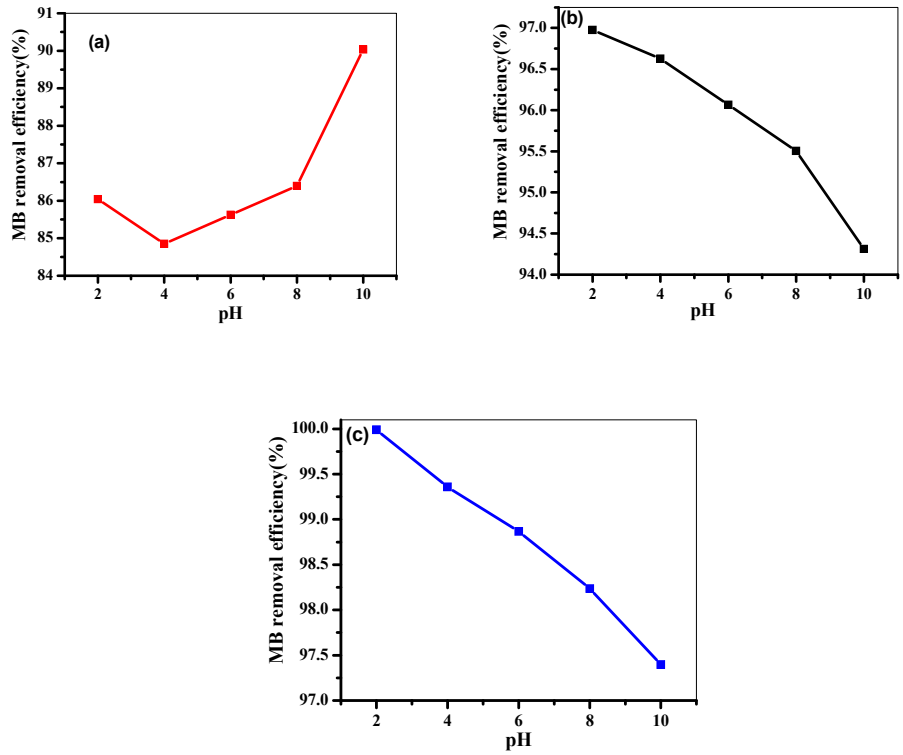

Fig. 7. Effect of pH on MB dye removal by (a) Ag NPs, (b) rGO, and (c) rGO/Ag NP nanocomposite adsorbent at 80 mg adsorbent dose, 10 mg/L initial concentration, 50 minute contact time and 310 rpm.

of MB by the selected Ag NPs, rGO, and rGO/Ag nanocomposite was shown in Figs. 8a, 8b, and 8c respectively. In all three adsorbents, the results indicate that the percentage removal of MB dye increased from 88.89% to 90.03% for Ag NPs, 96.27% to 96.97% for rGO, and 98.79% to 99.98% for rGO/Ag NPs nanocomposite with an increase of adsorbent amount up to 80 mg. This was due to an increase in adsorption sites. Further increases in the adsorbent dosage did not affect dye removal; it is due to the formation of aggregation and lack of dye molecules for the adsorption [41]. Thus, the optimum concentration of nanocomposite was found to be 80 mg, and this amount was used for further experimental analysis.

Effect of contact time

Equilibrium time is one of the most important variables in designing cost-effective systems for wastewater refinement. As shown in Figs. 9a, 9b, and 9c, the adsorption of methylene blue dye at an initial concentration of 10 mg/L was studied at different contact times (30–110 min) with an adsorbent dose of 80 mg for three synthesized adsorbents, Ag NPs at pH 10, rGO and rGO/Ag NCs at pH 2. Data showed that 50 minutes is sufficient to reach equilibrium conditions. The high adsorption rate in early contact times is due to several activated adsorption sites available for dye molecules that increase dye penetration to the adsorption surface. The concentration gradient decreases over time because of saturation of the adsorbent surface, and the removal percentage approximately remains constant.

At an initial 30 min up to the equilibrium time of 50 min of adsorption, the dye removal percentage was 88% to 90% for Ag NPs, 96.41% to 96.97% for rGO, and 98.86% to 99.98% for rGO/Ag NPs nanocomposite. As the time increases, the adsorption keeps on increasing and reaches equilibrium at 50 min with an adsorption efficiency of 99.98% for the nanocomposite adsorbent. This is due to the presence of a huge number of free adsorption sites during the initial stage of reaction, which then reduces as an increase in time and finally reaches equilibrium [42].

(cc) BY

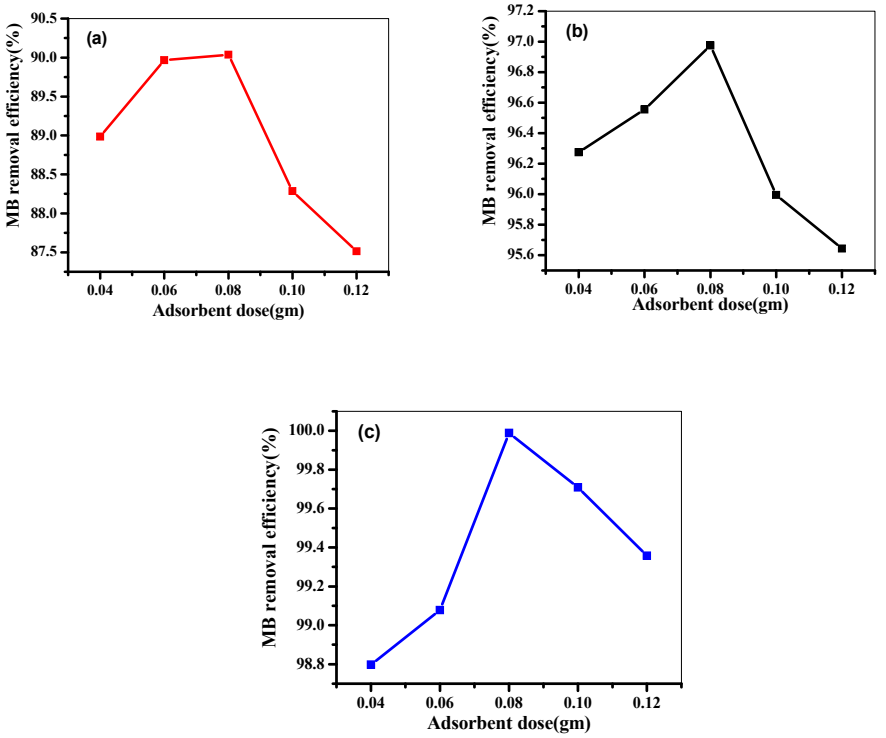

Fig. 8. Effect of adsorbent dose on the removal of MB dye by (a) Ag NPs, (b) rGO, and (c) rGO/Ag NP nanocomposite adsorbent at pH 10 for Ag NPs, pH 2 for rGO and rGO/Ag NPs, 10 mg/L initial concentration, 50 min contact time, and 310 rpm.

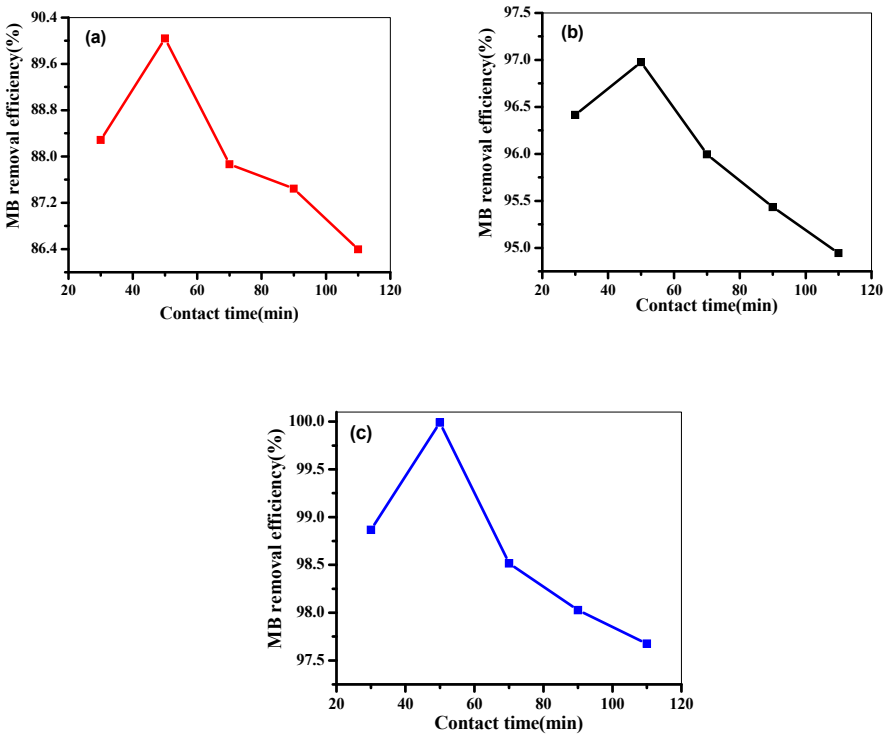

Fig. 9. Effect of contact time on the removal of MB dye by (a) Ag NPs, (b) rGO, and (c) rGO/Ag NP nanocomposite adsorbent at pH 10 for Ag NPs, pH 2 for rGO and rGO/Ag NPs, 10 mg/L initial concentration, and 310 rpm.

Effect of initial concentration

To investigate the effect of initial dye concentration on adsorption properties, a series of experiments were conducted using different concentrations of MB solution (10, 15, 20, and 25 mg/L) with an 80 mg adsorbent dose of Ag NPs, rGO, and rGO/Ag NPs nanocomposite at pH 10 for silver NPs and pH 2 for rGO and rGO/Ag nanocomposite within 50 min of contact time. As shown in Fig. 10, the adsorption was very fast at a lower initial concentration of MB solution.

The result revealed that removal efficiency was decreased with an increase in initial concentrations, although the amount of total MB accumulation increased. From this experiment, it was observed that about 90.03%, 96.97%, and 99.98% of MB were removed at an initial concentration of 10 mg/L by using Ag NPs, rGO, and rGO/Ag NPs nanocomposite adsorbents, respectively, at the same operating conditions shown in (Fig. 10a, 10b, and 10c). The percentage of MB removal decreases with an increase in the initial dye concentration, which may be due to the saturation of adsorption sites on the adsorbent surface. At a low initial concentration, there are unoccupied active sites on the adsorbent surface, so most of the MB solution might contact the active sites of adsorbents. However, at a higher concentration, most of the dye was not able to contact the active surfaces because the active sites might have been occupied by the MB solution, which is consistent with the results obtained [43].

Reusability test of rGO/Ag NP nanocomposite

The characteristic of a good adsorbent is to have both adsorptions as well as desorption capability that is of high efficiency. Fig. 11 shows the adsorption efficiency of rGO/Ag NPs nanocomposite at pH 2, time of 50 min and initial concentration of 10 mg/L was 99.98%, 96.55%, 92.35%, 87.79%, and 82.11% for first up to fifth cycle reusability, respectively. After five cycles, the adsorption efficiency of the nanocomposite remains more than 80%, which confirms that the synthesized rGO/Ag NP can act as a stable, efficient, and environmentally friendly adsorbent.

Adsorption isotherm

The adsorption isotherm indicates how retained particles diffuse between the liquid phase

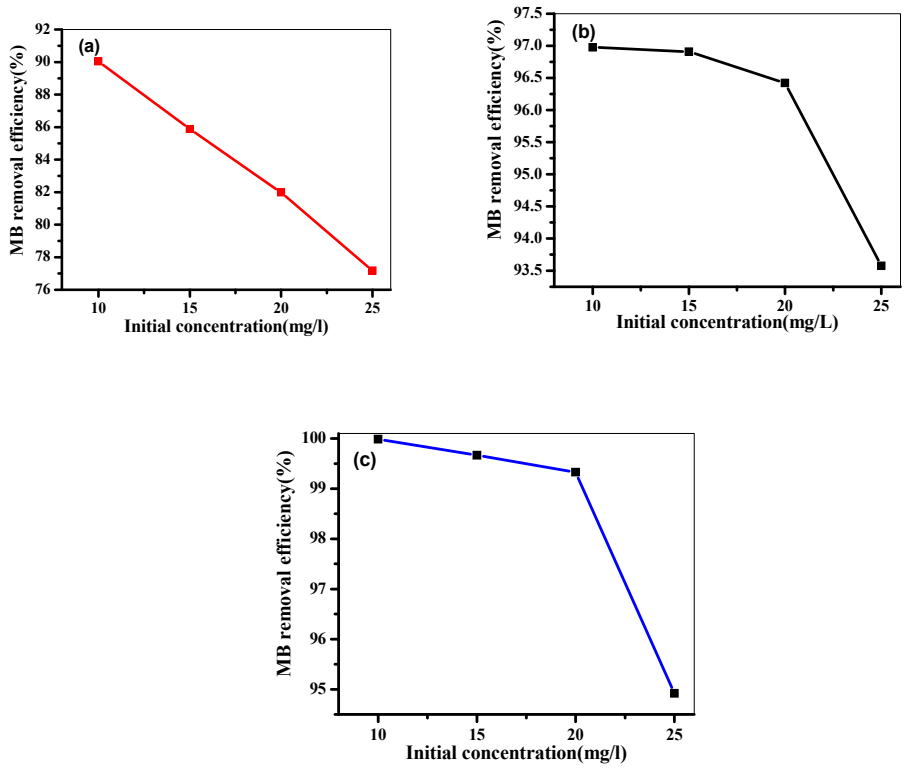

Fig. 10. Effect of initial concentration on MB dye removal by (a) Ag NPs, (b) rGO, and (c) rGO/Ag NP nanocomposite adsorbent at pH 10 for Ag NPs and pH 2 for rGO and rGO/Ag NPs, 80 mg adsorbent dose, 50 min contact time, and 310 rpm.

CC BY

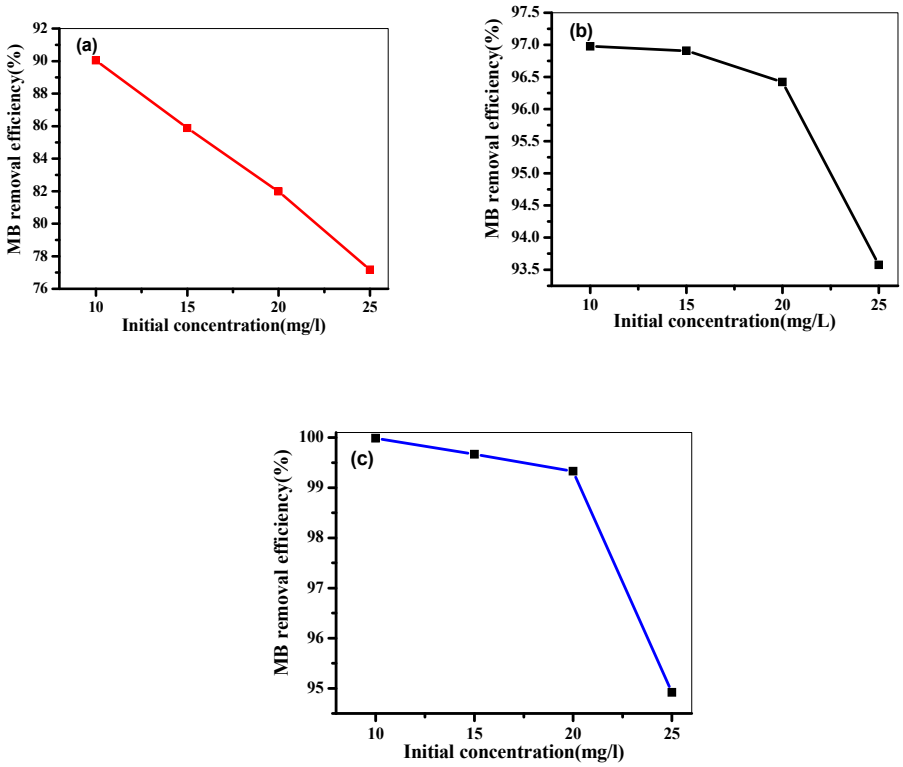

Fig. 11. Reusability test of rGO/Ag NP nanocomposite adsorbent for the removal of methylene blue dye.

and the solid surface when equilibrium is achieved during adsorption. The examination of the isotherm information by fitting them to various isotherm models is a vital step in finding an appropriate model. The adsorption isotherm model was limited to the synthesized Ag NPs, rGO, and rGO/Ag NPs nanocomposites adsorbents were explored with Freundlich and Langmuir adsorption isotherms.

Langmuir adsorption isotherm model

The Langmuir adsorption isotherm is based on the formation of homogeneous monolayer coverage on the adsorbent surface, uniform energy of adsorption, and no interaction between molecules adsorbed on neighboring sites [44]. The adsorption isotherms can be studied by determining the amount of dye adsorbed per unit mass of adsorbent (qe) and the concentration of dye in solution at equilibrium (Ce). In this, the Langmuir constant (K_L) and the maximum adsorption capacity (q_{max}) were obtained from the slope and the intercept of a linear form of the Langmuir equation, respectively [45].

$$\frac{\mathrm{Ce}}{\mathrm{qe}} = \frac{Ce}{q_{max}} + \frac{1}{q_{max}\,\mathrm{K_L}} \tag{9}$$

The values of q_{max} (mg/g) and K_L (L/mg) was determined from the plot of Ce vs Ce/qe. The adsorption capacity is often correlated with the variation in the area and porosity of the adsorbent. Higher surface area and pore volume resulted in higher adsorption capacity [46]. The essential characteristics of the Langmuir isotherm model are often expressed by a dimensionless constant called the equilibrium parameter, R_L.

The Langmuir adsorption was indicated by the maximum adsorption capacity (qmax), which represents the saturated monolayer adsorption at equilibrium. The result shown in Table 3 indicates the Langmuir adsorption isotherm parameters q_{max} (8.44 mg/g) and R^2 were 0.998 for silver nanoparticles, q_{max} (27.92 mg/g) and R^2 was 0.999 for reduced graphene oxide nanosheets, and q_{max} (763.35 mg/g) and R^2 was 0.999 for the rGO/Ag NPs nanocomposite. It indicates the correlation coefficient (R^2) and the q_{max} value of the nanocom-

Table 3. Parameters of Langmuir isotherm models for synthesized samples.

Langmuir isotherm model	synthesized samples		
	Ag NPs	rGO	rGO/Ag NPs NCs
q_{max} (mg/g)	8.44	27.92	763.35
R_L	0.05	0.11	0.83
K_L (L/mg)	1.87	0.11	0.01
R^2	0.998	0.999	0.999

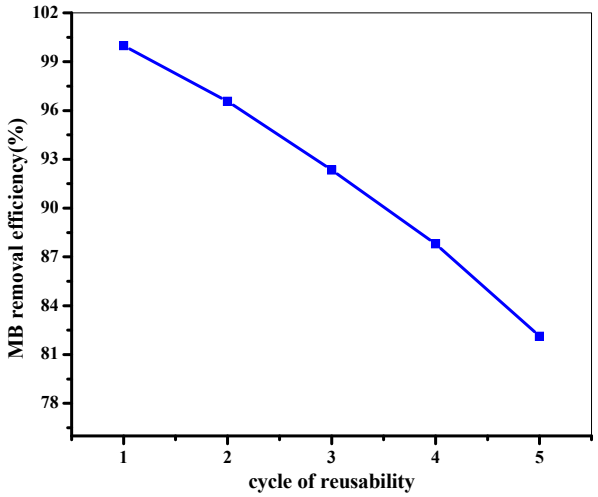

Fig. 12. Langmuir adsorption isotherm model of (a) Ag NPs, (b) rGO, and (c) rGO/Ag NPs NCs.

posite was better than the single precursor surface area by adsorption of methylene blue dye.

From the correlation coefficient R^2 of Langmuir, the adsorption isotherm indicates the adsorption study of MB dye on Ag NPs (Fig.12a), rGO, (Fig.12b), and rGO/Ag NPs nanocomposites (Fig.12c), were best fitted linearly by the Langmuir isotherm model. The calculated energy of adsorption constant a (K_L) values are 1.87 L/mg, 0.11 L/mg, and 0.01 L/mg for Ag NPs, rGO, and rGO/Ag NPs nanocomposite, respectively. This indicated that the adsorption efficiency of the three adsorbents was good, but the nanocomposite was better than the other two because its K_L value was smaller. According to the Langmuir model, the R_L values calculated as 0.05, 0.11, and 0.833 were obtained between 0 and 1 for Ag NPs, rGO, and rGO/Ag NPs nanocomposite, respectively, which confirmed that the adsorbents adsorbing MB from aqueous solution are favorable under the conditions applied in this study.

Freundlich adsorption isotherm model

The Freundlich adsorption isotherm is based on the formation of a heterogeneous surface or surfaces supporting sites of varied affinities, and it is assumed that the stronger binding sites are occupied first and that the binding strength decreases with an increasing degree of site occupation. The Freundlich isotherm model best describes the cases of non-ideal and reversible adsorption, which are not restricted to the formation of a monolayer. This empirical model can be applied to multilayer adsorption with a non-uniform distribution of adsorption heat and affinities over the heterogeneous surface [47]. The linear form of the Freundlich isotherm equation is as follows:

$$\ln \mathrm{qe} = \ln Kf + \frac{1}{n} * \ln Ce \qquad (10)$$

A smaller value of the Freundlich equation coefficient 1/n points to a better adsorption mechanism and the formation of a relatively stronger bond between adsorbate and absorbent. Bond energies increase with surface density if 1/n = 1, decrease with surface density if 1/n > 1, and all

CC BY

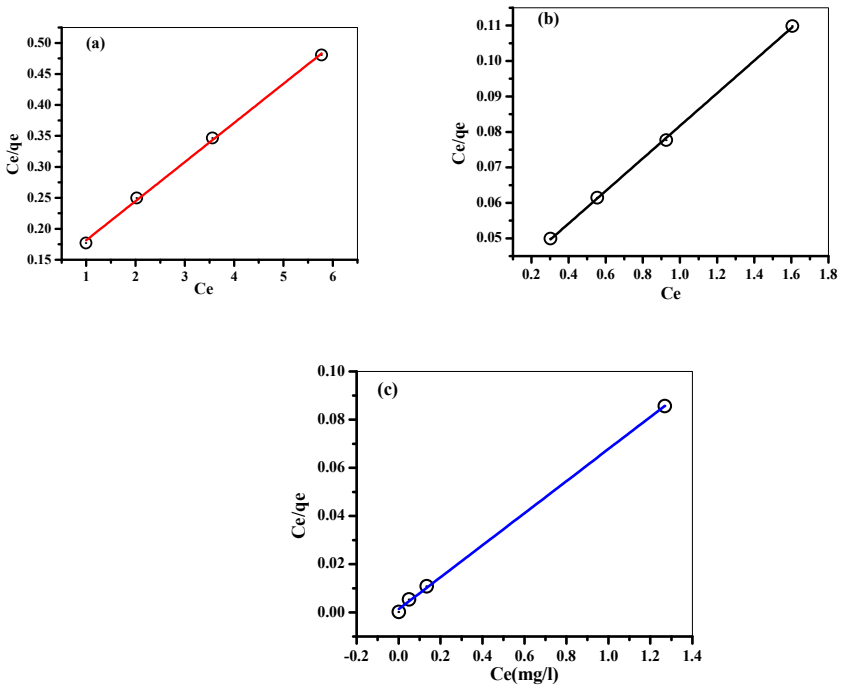

Fig. 13. Freundlich adsorption isotherm models for Ag NPs (a), rGO (b), and rGO/Ag NPs NCs (c).

Table 4. Freundlich isotherm model parameters for synthesized samples.

Freundlich isotherm model	synthesized samples		
	Ag NPs	rGO	rGO/Ag NPs NCs
K_F (mg/g)	5.78	11.87	14.67
(n)	2.30	1.88	7.90
1/n	0.43	0.53	0.12
R^2	0.985	0.976	0.955

Table 5. Parameters of pseudo-1st order and pseudo-2nd order for synthesized samples.

	Ag NPs		rGO		rGO/Ag NPs NCs	
	Pseudo-1st order	Pseudo-2nd order	Pseudo-1st order	Pseudo 2nd-order	Pseudo -1st order	Pseudo-2nd order
qe(experimental)	5.62	5.62	6.06	6.06	6.24	6.24
qe(calculated)	0.08	5.40	0.001	5.93	0.0921	6.10
R^2	0.3314	0.9994	0.3249	0.9998	0.3196	0.9998

surface sites are equivalent if 1/n = 1. The n values lie in the range of 1–10 for classification as favorable adsorption [48].

The Freundlich adsorption isotherms of AgNPs, rGO, and rGO/AgNPs were presented in Fig. 13a, Fig 13b and Fig. 13c respectively. The isotherm result are also summarized in Table 4.5 as the Freundlich parameter, of 1/n value, was between 0 & 1, which indicates the favorability of MB dye adsorption on Ag NPs, rGO, and rGO/Ag NPs nanocomposite adsorbent. This means the value of (n) is greater than 1, which indicates the bond between the MB dye and the three synthesized adsorbents was strong. In this study, the calculated values of Freundlich equation coefficient n (n = 2.30 for Ag NPs, 1.88 for rGO nanosheets, and 7.90 for rGO/Ag NPs nanocomposite adsorbent) were greater than 1, which indicates that the adsorption process is

favorable. From the Freundlich constant (K_F) values of rGO/Ag, NPs nanocomposite adsorbent was found to be better than Ag NPs and rGO. This is because the high value of K_F shows that the high adsorption rGO/Ag NPs NCs (14.67) is greater than Ag NPs (5.78) and rGO (11.87). In addition, the correlation coefficient R^2 of Freundlich was 0.985, 0.976, and 0.955 for Ag NPs, rGO, and rGO/Ag NPs nanocomposite adsorbents, respectively. This indicates the Freundlich isotherm correlation coefficient R^2 was lower than the Langmuir isotherm correlation coefficient of the three adsorbents. So this indicates the Langmuir isotherm model is better fitted for methylene blue dye adsorption for the three synthesized samples. The values of the constants and calculated parameters of the Freundlich isotherm are shown in Table 4.

Adsorption kinetic studies

Several kinetics models can be employed to evaluate the rate and mechanism of mass transfer of MB from the liquid phase to the surface of adsorbents. In the present study, the pseudo-first-order and pseudo-second-order kinetic models were adopted to understand the adsorption mechanism of MB to the three different adsorbents. The pseudo-first-order model was described by Lagergren (1898) in a linear form as displayed in the equation, and the linear form of the pseudo-second-order model was summarized by Ho and McKay (1999) as written in the equation below.

$$\ln\left(\mathrm{qe}-\mathrm{qt}\right)=lnqe+K_1t \tag{11}$$

$$\frac{\mathrm{t}}{\mathrm{qt}}=\frac{1}{K_2qe^2}+\frac{t}{qe} \tag{12}$$

Where qe and qt represent the adsorption capacities (mg/g) at equilibrium and at time t, respectively, and k_1 (min^{-1}) and k_2 (gmg^{-1} min^{-1}) are the corresponding rate constants.

Pseudo-first order kinetics

The linear curves plotted based on pseudo-first-order and pseudo-second-order kinetics models are given in Fig. 14, and the values of qe, k_1, k_2, and R^2 are summarized in Table 4.6. The kinetics of MB adsorption onto Ag NPs, rGO, and rGO/Ag NPs nanocomposite were analyzed using

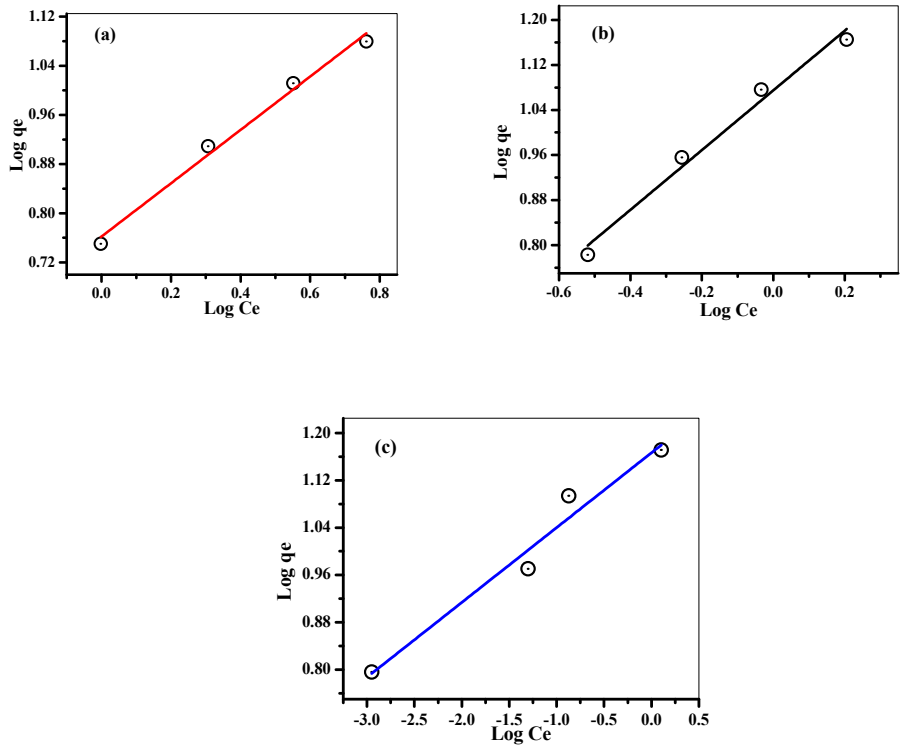

Fig. 14. pseudo second-order models of (a) Ag NPs, (b) rGO, and (c) rGO/Ag NPs NCs.

(cc) BY

a pseudo-first-order kinetic model. The conformity between experimental data of Ag NPs was (5.62) and the calculated value (0.08), for rGO q_{exp} (6.06), q_{cal} (0.001), and for rGO/Ag NPs nanocomposite q_{exp} (6.24), q_{cal} (0.09) shows disagreement and also that the correlation coefficient R^2 was not close to unity, therefore it is not a favorable model for the adsorption of MB onto the adsorbents as shown in Table 5 [49].

Pseudo-second order kinetics

A pseudo-second-order kinetic model explains the adsorption mechanism over the entire contact time range. The plot of the kinetic model was presented in Figs. 14a, 14b and 14 c for AgNPs, rGO, and rGO/AgNPs nanocomposite respectively. The calculated adsorption capacity from the pseudo-second-order model (5.40 mg/g) is closer to experimental data (5.62 mg/g) for Ag NPs, q_{cal} (5.93 mg/g) is closer to q_{exp} (6.06 mg/g) for rGO nanosheets, and q_{cal} (6.10 mg/g) was closer to q_{exp} (6.24 mg/g) for rGO/Ag NPs nanocomposite adsorbent than that of the pseudo-first-order model (Table 5). Furthermore, the comparison of the two kinetics correlation coefficients (R^2) also demonstrates that the adsorption process of MB from an aqueous solution fits the pseudo-second-order model better. As shown in Table 5, the correlation coefficient was found to be closer to unity in the case of the pseudo-second-order kinetic model (0.9994, 0.9998, and 0.9998), which is higher than that of the pseudo-first-order kinetic model (0.331, 0.324, and 0.319) for Ag NPs, rGO, and rGO/Ag NPs NCs, respectively which confirms that the experimental adsorption data for all cases best fits the pseudo-second -order kinetic model [50].

CONCLUSION

The current study provides a feasible immobilization of green synthesized Ag NPs, rGO, and rGO/Ag NCs using a reduction process using cinnamon bark aqueous extract as a reductant and stabilizer. Diverse techniques (UV-DRS, FTIR-ATR, SEM, and XRD) have been used to characterize the three synthesized adsorbents.

The XRD results showed that the average particle sizes were 29.9 nm, 0.67 nm, and 13.35 nm for Ag NPs, rGO, and rGO/Ag NPs nanocomposite respectively. The synthesized rGO/Ag nanocomposite solid samples used for the removal of MB dye from the aqueous solution better than Ag NPs, and rGO. The removal efficiency of rGO/Ag nanocomposite was 99.98%, while Ag NP and rGO nanosheets removal efficiency were 90.03% and 96.97% respectively. The adsorption results indicate that rGO/Ag nanocomposites are highly capable of removing MB and displaying a high adsorption potential of up to 763.35 mg/g but in the case of Ag NPs, q_{max} was 8.44, for rGO, q_{max} was 27.42 mg/g. In the adsorption process, different parameters affect the efficiency like pH, adsorbent dose, contact time, and initial MB concentration. These parameters were optimized for the three different adsorbent methylene blue removals from an aqueous solution. The adsorption data was compatible with the Langmuir model because their R^2 values were close to unity than the Freundlich isotherm model. From the kinetic study, the adsorption process pursued a pseudo-second-order model because their R^2 value was close to unity and the graph line touched all points. The rGO/Ag NPs nanocomposite also had good reusability efficiency for a five consecutive adsorption process; its removal efficiency was greater than 82%. Thus, this study confirms that the rGO/Ag NP composite is an effective adsorbent for the removal of dye pollutants.

ACKNOWLEDGEMENT

The authors would like to thank the financial support from Adama Science and Technology University, Ethiopia.

AUTHOR CONTRIBUTIONS

Bekele Yirga

designed the methodology, conducted the experiments, performed the data analysis, and wrote the original draft.

Tegene Desalegn

involved in methodology design, performed the data analysis & interpretation, reviewed and edited the article.

DISCLOSURE STATEMENT

No conflict of interest was accounted by the authors.

REFERENCES

1. Crini G., Lichtfouse E., Chanet G., Morin-Crini N., (2020), Applications of hemp in textiles, paper industry, insulation and building materials, horticulture, animal nutrition, food and beverages, nutraceuticals, cosmetics and hygiene, medicine, agrochemistry, energy production and environ-

ment. *Environ. Chem. Lett.*18: 1451-1476.
2. Jemal A. F., Fangnon Firmin Rejoice F., (2020), Effectiveness assessment of industrial effluent standard implementation in Addis Ababa city, Ethiopia. *Int. J. Sci. Res. Pub.* 10: 141-148.
3. Menbere M. P., Menbere T. P., (2019), Industrial wastes and their management challenges in Ethiopia. *Institutions*. 11: 1-6.
4. Konicki W., Aleksandrzak M., Mijowska E., (2017), Equilibrium, kinetic and ther-modynamic studies on adsorption of cationic dyes from aqueous solutions using graphene oxide. *Chem. Eng. Res. Des*. 123: 35-49.
5. Guarín J. R., Moreno-Pirajan J. C., Giraldo L., (2018), Kinetic study of the bioadsorption of methylene blue on the surface of the biomass obtained from the algae D. Antarctica. *J. Chem*. 2018: 1-12.
6. Aboubaraka A. E., Aboelfetoh E. F., Ebeid E. Z. M., (2017), Coagulation effectiveness of graphene oxide for the removal of turbidity from raw surface water. *Chemosphere*. 181: 738-746.
7. Fu L., Fu Z., (2015), Plectranthus amboinicus leaf extract assisted biosynthesis of ZnO nanoparticles and their photocatalytic activity. *Ceram. Int.* 41: 2492–2496.
8. Sreeprasad T. S., Maliyekkal S. M., Lisha K. P., Pradeep T., (2011), Reduced graphene oxide–metal/metal oxide composites: Facile synthesis and application in water purification. *J. Hazard Mater.* 186: 921–931.
9. Fei P., Zhong M., Lei Z., Su B., (2013), One-pot solvothermal synthesized enhanced magnetic zinc ferrite-reduced graphene oxide composite material as adsorbent for methylene blue removal. *Mater. Let.* 108: 72-74.
10. Choi B.-hee., Lee H.-H., Jin S., Chun S., Kim S.-H., (2007), Characterization of the optical properties of silver nanoparticle films. *Nanotechnol.* 18: 075706-075710.
11. Lu Y., Mei Y., Schrinner M., Ballauff M., Möller M. W., Breu J., (2007), In situ formation of Ag nanoparticles in spherical polyacrylic acid brushes by UV irradiation. *J. Phys. Chem. C*. 111: 7676-7681.
12. Vidhu V. K., Philip D., (2014), Catalytic degradation of organic dyes using biosynthesized silver nanoparticles. *Micron*. 56: 54-62.
13. Azeez L., Lateef A., Adebisi S. A., Oyedeji A. O., (2018), Novel biosynthesized silver nanoparticles from Cobweb as adsorbent for rhodamine B: Equilibrium Isotherm, kinetic and thermodynamic studies. *Appl. Water Sci.* 8: 1-12.
14. Azizi Lalabadi M., Hashemi H., Feng J., Jafari S. M., (2020), Carbon nanomaterial against pathogens; the antimicrobial activity of carbon nanotubes, graphene/graphene oxide, fullerenes, and their nanocomposites. *Adv. Colloid Interf. Sci.* 284: 102250-102256.
15. Nabavi S., di Lorenzo A., Izadi M., Sobarzo Sánchez E., Daglia M., Nabavi S., (2015), Antibacterial effects of cinnamon: From farm to food, cosmetic and pharmaceutical industries. *Nutrients*. 7: 7729-7748.
16. Moosavi R., Ramanathan S., Lee Y. Y., Siew Ling K. C., Afkhami A., Archunan G., Padmanabhan P., Gulyás B., Kakran M., Selvan S. T., (2015), Synthesis of antibacterial and magnetic nanocomposites by decorating graphene oxide surface with metal nanoparticles. *RSC Adv.* 93: 76442-76450.
17. Suresh D., Udayabhanu P. K. M., Nagabhushana H., Sharma S., (2015), Cinnamon supported facile green reduction of graphene oxide, its dye elimination and antioxidant activities. *Mater. Lett*. 151: 93-95.
18. Supritha C. T., (2021), Green synthesis and characterization of silver nanoparticles using *cinnamomum zeylanicum bark* extract. *Int. J. Curr. Microbiol. Appl. Sci.* 10: 444-451.
19. Ghareeb M. A., Habib M. R., Mossalem H. S., Abdel-Aziz M. S., (2018), Phytochemical analysis of *eucalyptus camaldulensis* leaves extracts and testing its antimicrobial and schistosomicidal activities. *Bull. Nati. Res. Cent*. 42: 1-9.
20. IK M., Uthman ISAH K., (2015). The effect on extracting solvents using natural dye extracts from hyphaene thebaica for dye sensitized solar cells. *Mater. Sci. Eng.* 5: 119-125.
21. Dandjesso C., (2012), Phytochemistry and hemostatic properties of some medicinal plants sold as anti-hemorrhagic in Cotonou Markets (Benin). *Ind. J. Sci. Technol*. 5*:* 1–5.
22. Sofowora A., (1996), Research on medicinal plants and traditional medicine in Africa. *J. Alter. Complement. Med*. 2: 365-372.
23. Mulushewa Z., Dinbore W. T., Ayele Y., (2021), Removal of methylene blue from textile waste water using kaolin and zeolite-x synthesized from Ethiopian kaolin. *Environ. Anal. Health Toxicol.* 36: 23-28.
24. Markandeya Shukla S. P., Dhiman N., Mohan D., Kisku G. C., Roy S., (2017), An efficient removal of disperse dye from wastewater using zeolite synthesized from cenospheres. *J. Hazard. Toxic Radioact. Waste*. 21: 04017017.
25. Yuan N., Cai H., Liu T., Huang Q., Zhang X., (2019), Adsorptive removal of methylene blue from aqueous solution using coal fly ash-derived mesoporous silica material. *Adsorpt. Sci. Technol.* 37: 333-348.
26. Paliwal R., Sharma V., Sharma S., (2011), Elucidation of free radical scavenging and antioxidant activity of aqueous and hydro-ethanolic extracts of Moringa oleifera pods. *Rese. J. Pharm Technol*. 4: 566-571.
27. Ebana R., Edet U., Ekanemesang U., Etok C., Ikon G., Noble M., (2016), Phytochemical screening and antimicrobial activity of three medicinal plants against urinary tract infection pathogens. *Asian J. Med. Health*. 1: 1–7.
28. Ibrahim H. M. M., (2015), Green synthesis and characterization of silver nanoparticles using banana peel extract and their antimicrobial activity against representative microorganisms. *J. Radiat. Res. Appl. Sci*. 8: 265–275.
29. Hemmati S., Heravi M. M., Karmakar B., Veisi H., (2020), Green fabrication of reduced graphene oxide decorated with Ag nanoparticles (rGO/Ag NPs) nanocomposite: A reusable catalyst for the degradation of environmental pollutants in aqueous medium. *J. Mol. Liq*. 319: 114302.
30. Gawade V. V., Gavade N. L., Shinde H. M., Babar S. B., Kadam A. N., Garadkar K. M., (2017), Green synthesis of ZnO nanoparticles by using Calotropis Procera leaves for the photo degradation of methyl orange. *J. Mater. Sci. Mater. Elec*. 28: 14033-14039.
31. Singaravelan R., Bangaru Sudarsan Alwar S., (2015), Electrochemical synthesis, characterization and phytogenic properties of silver nanoparticles. *Appl. Nanosci*. 5: 983–991.
32. Bai R. G., Muthoosamy K., Shipton F. N., Pandikumar A., Rameshkumar P., Huang N. M., Manickam S., (2016), The biogenic synthesis of a reduced graphene oxide-silver (rGO-Ag) nanocomposite and its dual applications as an antibacterial agent and cancer biomarker sensor. *RSC Adv.*

CC BY

43: 36576-36587.
33. Jeon J.-W., Jeon D.-W., Sahoo T., Kim M., Baek J.-H., Hoffman J. L., Kim N. S., Lee I.-H., (2011), Effect of annealing temperature on optical band-gap of amorphous indium zinc oxide film. *J. Alloy Compd.* 509: 10062–10065.
34. Lu X. M., Zhu J. S., Zhang W. Y., Ma G. Q., Wang Y. N., (1996), The energy gap of rf-sputtered $BaTiO_3$ thin films with different grain size. *Thin Solid Films*. 274*:* 165–168.
35. Kim B. S., Salunke B., Sawant S., Alkotaini B., (2014), Biological synthesis of silver nanoparticles using plant leaf extracts and their specific antimicrobial activity. *New Biotechnol.* 31: 125-129.
36. Lee S., Jun B.-H., (2019), Silver nanoparticles: Synthesis and application for nanomedicine. *Int. J. Mol. Sci*. 20*:* 865-869.
37. Theivasanthi T., Alagar M., (2012), Electrolytic synthesis and characterization of silver nanopowder. *Nano Biomed. Eng.* 4: 112-118.
38. Singh S., Joshi M., Panthari P., Malhotra B., Kharkwal A. C., Kharkwal H., (2017), Citrulline rich structurally stable zinc oxide nanostructures for superior photo catalytic and optoelectronic applications: A green synthesis approach. *Nano-Struct. Nano-Objects*. 11: 1–6.
39. Mangalam J., Kumar M., Sharma M., Joshi M., (2019), High adsorptivity and visible light assisted photocatalytic activity of silver/reduced graphene oxide (Ag/rGO) nanocomposite for wastewater treatment. *Nano-Struct. Nano-Objects*. 17: 58–66.
40. Das S. K., Khan M. M., Parandhaman T., Laffir F., Guha A. K., Sekaran G., Mandal A. B., (2013), Nano-silica fabricated with silver nanoparticles: Antifouling adsorbent for efficient dye removal, effective water disinfection and biofouling control. *Nanoscale*. 5: 5549-5553.
41. Wu Q., Feng C., Wang C., Wang Z., (2013), A facile one-pot solvothermal method to produce superparamagnetic graphene–Fe_3O_4 nanocomposite and its application in the removal of dye from aqueous solution. *Colloids Surf. B.* 101: 210–214.
42. Elmorsi T. M., (2011), Equilibrium isotherms and kinetic studies of removal of methylene blue dye by adsorption onto Miswak leaves as a natural adsorbent. *J. Environ. Prot.* 02: 817-827.
43. Rahman M. A., Amin S. M., Alam A. M., (2012), Removal of methylene blue from waste water using activated carbon prepared from rice husk. *Dhaka Univ. J. Sci.* 60: 185–189.
44. Gemeay A. H., Elsharkawy R. G., Aboelfetoh E. F., (2017), Graphene Oxide/Polyaniline/Manganese Oxide Ternary nanocomposites, facile synthesis, characterization, and application for indigo carmine removal. *J. Polym. Environ.* 26: 655–669.
45. Md Sandollah N. A., Sheikh Mohd Ghazali S. A., Wan Ibrahim W. N., Rusmin R., (2020), Adsorption-desorption profile of methylene blue dye on raw and acid activated kaolinite. *Indones. J. Chem.* 20: 755-765.
46. Kavithad D., Namasivayam C., (2007), Experimental and kinetic studies on methylene blue adsorption by Coir Pith Carbon. *Bioresource Technol.* 98*:* 14–21.
47. Wang H., Yuan X., Zeng G., Leng L., Peng X., Liao K., Peng L., Xiao Z., (2014), Removal of malachite green dye from wastewater by different organic acid-modified natural adsorbent: Kinetics, equilibriums, mechanisms, practical application, and disposal of dye-loaded adsorbent. *Environ. Sci. Pollut. Res.* 21: 11552–11564.
48. Salifu A., (2017), Fluoride removal from drinking water using granular aluminum-coated bauxite as adsorbent: Optimization of synthesis process conditions and equilibrium study. *Fluoride Remov. Groundwater Adsorp. Technol.* (pp.161–202). *CRC Press.*
49. Hermawan A. A., Bing T. K., Salamatinia B., (2015), Application and optimization of using recycled pulp for methylene blue removal from wastewater: A response surface methodology approach. *Int. J. Environ. Sci. Dev.* 6: 267–274.
50. Jaseela P. K., Garvasis J., Joseph A., (2019), Selective adsorption of methylene blue (MB) dye from aqueous mixture of MB and methyl orange (MO) using mesoporous titania (TiO_2)-poly vinyl alcohol (PVA) nanocomposite. *J. Mol. Liq.* 286: 110908-110912.